Published in final edited form as:
*Mol Pharm*. 2008 ; 5(2): 287–293. doi:10.1021/mp7001158.

# New Ways of Imaging Uptake and Intracellular Fate of Liposomal Drug Carrier Systems inside Individual Cells, Based on Raman Microscopy

**Christian Matthäus**[†], **Amit Kale**[‡], **Tatyana Chernenko**[†], **Vladimir Torchilin**[*,‡], and **Max Diem**[*,†]

[†]Department of Chemistry and Chemical Biology, Northeastern University, Boston, Massacusetts 02115

[‡]Department of Pharmaceutical Sciences and Center for Pharmaceutical Biotechnology and Nanomedicine, Northeastern University, Boston, Massacusetts 02115

## Abstract

Recent developments, combining Raman spectroscopy with optical microscopy, provide a new noninvasive technique to assess and image cellular processes. Of particular interest are the uptake mechanisms of various cytologically active compounds. In order to distinguish the species of interest from their cellular environment spectroscopically, compounds may be labeled with deuterium. Here, we apply Raman microspectroscopy to follow the uptake of liposomal drug carrier systems that have been introduced to deliver biologically active compounds to their site of action within human breast adenocarcinoma MCF-7 cells. The distribution patterns of liposomes and liposomes surface-modified with a cell-penetrating peptide (TAT-peptide, TATp) have been imaged over time. The spectroscopic information obtained provides a clear evidence for variable rates, as well as different efficiencies of liposome uptake depending on their surface properties. Depending on the experimental setup, the technique may be applied to fixed or living cell organisms.

### Keywords

Liposomes; Raman imaging; drug delivery; cells

## Introduction

Microscopic imaging of subcellular organelles and their functioning provides a crucial insight into the details of cellular biology. A currently common technique to image cellular processes is fluorescence microscopy. Fluorescence may be emitted either by molecules that are intrinsically fluorescing or by introducing fluorescence dyes or labels. Although the technique is well established, there are certain difficulties encountered, such as low contrast and photobleaching. In addition, the introduction of the fluorescent label may potentially alter the biochemical properties of the molecules of interest. With the recent development of microscopic imaging techniques, based on vibrational optical spectroscopy, novel means



*To whom correspondence should be addressed. (V.T.) Mailing address: Department of Pharmaceutical Sciences and Center for Pharmaceutical Biotechnology and Nanomedicine, Northeastern University, 360 Huntington Ave, Mugar Hall, Room 312, Boston, MA 02115. Tel: 617-373-3206. Fax: 617-373-4201. E-mail: E-mail: v.torchilin@neu.edu. (M.D.) Mailing address: Department of Chemistry and Chemical Biology, 360 Huntinton Ave, Hurtig Hall, Room 316, Boston, MA 02115. Tel: 617-373-2922. Fax: 617-373-8795. E-mail: E-mail: m.diem@neu.edu.

appeared to characterize subcellular structures. Molecular vibrations may be excited either by infrared radiation or nonelastic scattering of photons, which is commonly known as the Raman effect. Since the spatial resolution is related to the wavelength of the incoming light, the latter technique, usually referred to as Raman microspectroscopy, is more feasible for the imaging on the subcellular level. The technique offers the possibility to image structures based on their vibrational properties and thus their chemical composition, bypassing the need for any staining procedures. It has been demonstrated that Raman microspectroscopy is capable of imaging cellular organelles such as the nucleus or chromatin,[1,2] mitochondria,[3] and lipid bodies,[4,5] as well as following metabolic processes or enzymatic activity inside cells.[6–8]

Apart from imaging subcellular features, Raman imaging may provide an opportunity to follow the uptake of molecules in cell cultures. One way to distinguish incorporated molecules inside cells is to use deuterated compounds.[4] As long as the deuterium is covalently bound to the molecule of interest, this approach is nonperturbing and may also be applied to cells that are kept alive.

We have made an attempt to use the technique to investigate the cellular uptake and intracellular fate of liposomal nanocarriers. Currently, liposomes are widely used for drug delivery purposes,[9] including intracellular drug and gene delivery.[10,11] Although important information regarding the uptake kinetics of liposomes by cells as well their intracellular distribution and degradation is obtained by applying various techniques, such as small-angle X-ray spectroscopy,[11] fluorescence microscopy,[12] flow cytometry, and spectral bioimaging,[13] many issues related to fine mechanisms of the liposome-to-cell interaction remain unresolved. This is especially true for the case of intracellular delivery of liposomal nanocarriers, which are modified by cell-penetrating peptides, such as HIV-1 trans-activating transcriptional activator-derived TAT peptide.[14] These carrier systems are currently considered as a very promising way to bring various drugs including protein and peptide drugs into cells.[15] Many cytotoxic compounds cannot exert their biological activity because they fail to pass the membrane. On the other hand, those compounds that are taken up by cells via endocytosis often end in the cell's lysosomes, where they undergo significant biodegradation. To bypass the problem, a number of drug delivery systems have been developed, which are internalized by TAT peptide-mediated transduction mechanism. Once inside the cell, different cell organelles may be targeted, depending on the nature of the disease. Vectors for gene therapy have to be delivered to the nuclei, proapoptotic drugs have to reach the mitochondria, or drugs affecting lysosomal enzymes have to be incorporated into lysosomal compartments.[16] Thus, one of the key issues is the fate of the liposomal drug carriers once they have passed the membrane.

Here, we demonstrate the feasibility of Raman imaging to follow the uptake of deuterated liposomes and to compare the uptake of "plain" and TAT peptide-modified liposomes. With this in mind, two liposomal systems based on 1,2-distearoyl-d70-*sn*-glycero-3-phosphocholine (DSPC-$d_{70}$), in which the hydrogen atoms of the two distearoyl side chains are exchanged by deuterium, were investigated-plain DSPC-$d_{70}$ liposomes (LIP) and TAT peptide-modified DSPC-$d_{70}$ liposomes (TATp-LIP).

## Experimental Section

### Raman Data Acquisition

Raman spectra were acquired using a WITec, Inc. (Ulm, Germany) model CRM 2000 Confocal Raman Microscope. Excitation (ca. 30 mW at 488 nm) is provided by an air-cooled Ar ion laser (Melles Griot, model 532). The exciting laser radiation is coupled into a Zeiss microscope through a wavelength-specific single mode optical fiber. The incident laser beam is collimated via an achromatic lens and passes a holographic band-pass filter before it is focused onto the

sample through the microscope objective. A Nikon Fluor (60×/1.00 NA, WD = 2.0 mm) water immersion objective was used in the studies reported here.

The sample is located on a piezo-electrically driven microscope scanning stage with an *x*,*y* resolution of ca. 3 nm and a repeatability of ±5 nm and *z* resolution of ca. 0.3 nm and ±2 nm repeatability. The sample is scanned through the laser focus in a raster pattern at a constant stage speed of fractions of a micrometer per second. The continuous motion prevents sample degradation at the focal point of the laser beam. Spectra are collected at a 0.5 μm grid, with a dwell time of 0.5 s.

Raman back-scattered radiation is collected through the microscope objective and passes a holographic edge filter to block Rayleigh scattering and reflected laser light before being focused into a multimode optical fiber. The 4 μm diameter single-mode input fiber and the 50 μm diameter multimode output fiber provide the optical apertures for the confocal measurement. The light emerging from the output optical fiber is dispersed by a 30 cm focal length, f/4 Czerny-Turner monochromator, incorporating interchangeable gratings (1800/mm, blazed at 500 nm and 600/mm, blazed at 500 nm). The light is finally detected by a back illuminated deep-depletion, 1024 × 128 pixel CCD camera operating at − 82 °C. Spectral resolution depends on the excitation wavelength and grating groove density; for 488 nm excitation and the 600/mm grating, the optical resolution varies from about 5.5 $cm^{-1}$/ data at about 200 $cm^{-1}$ to about 3.3 $cm^{-1}$/ data point at 4500 $cm^{-1}$.

## Preparation of Liposomes

1,2-Distearoyl-$d_{70}$-*sn*-glycero-3-phosphocholine (DSPC-$d_{70}$) was obtained from Avanti Polar Lipids, Inc. (Alabaster, AL). Plain liposomes were prepared from DSPC-$d_{70}$ by the lipid film hydration method.[17,18]The dried lipid film prepared from the chloroform solution of DSPC-$d_{70}$ was hydrated and vortexed with HEPES-buffered saline (HBS), pH 7.4, at DSPC-$d_{70}$ concentration of 1.6 mM. The resulting liposomes were sized through double-stacked 200 nm pore size polycarbonate membranes (Nucle-opore) using a hand-held extruder (Avanti). The liposome size was monitored by using a Coulter N4 MD Submicron Particle Size Analyzer (Coulter Electronics).

## Preparation of TATp-liposomes

Purified TATp was received from Tufts University Core Facility (Boston, MA). For preparing TATp-liposomes, TATp-$PEG_{3400}$-PE was added to the lipid film. The hydration and sizing of TATp-liposomes were done as described above. TATp-$PEG_{3400}$-PE was prepared by reacting TATp with *p*-nitrophenyl carbonyl-$PEG_{3400}$-DOPE (pNP-PEG-PE).[19] Briefly, pNP-PEG-PE film was hydrated with a citrate buffer, pH 5.0 (10 mM sodium citrate, 150 mM sodium chloride), at 0.95 mM concentration. TATp was dissolved in a borate buffer, pH 9.2 (100 mM sodium borate, 140 mM NaCl), and mixed at 1.7 molar excess of pNP-PEG-PE. The mixture was incubated with stirring overnight at rt followed by further incubation for 1 day at 4 °C. During the incubation, TATp gets attached to the distal ends of pNP-PEG-PE yielding loose micelles of TATp-PEG-PE. TATp-PEG-PE was purified by dialysis against PBS, pH 8.0 (dialysis tubing cut off size of 12 000 Da) for 1 day and then against water for 2 days at 4 °C. TATp-PEG-PE was dried under a freeze-dryer and dissolved in chloroform for storage at −80 °C until use.

## Cell Culture and Incubation

Human breast adenocarcinoma MCF-7 cells (cell line HTB-22, ATCC, Manassas, VA) were grown in Eagle's Minimum Essentials Medium (MEM, ATCC), supplemented 10% fetal bovine serum (FBS, ATCC), and incubated at 37 °C in 5% $CO_2$ atmosphere. The cells were fixed in a 10% phosphate-buffered formalin solution (Sigma-Aldrich, St. Louis, MO) and

washed in phosphate-buffered saline. To avoid scattering from the surface of regular glass windows, Raman data were acquired of cells grown onto optically flat $CaF_2$ windows (Wilmad LabGlas, Buena, NJ), which were submerged in buffer solution during the measurement.

Incubations with liposomes were carried out at 37 °C, well below the pre- and main transition temperatures, which have been determined to be 47.8 and 54.4 °C, respectively.[20] All Raman measurements were performed at room temperature. The osmolality of the culture medium used was 290 ± 30 mOsm (MEM, Mediatech, Inc., Manassas, VA).

## Results

Human breast adenocarcinoma MCF-7 cells were incubated for different time intervals with deuterated LIP and TATp-LIP at lipid concentration of 2 mg/mL for both carrier systems. After the incubation, the cells where fixed in a formalin-phosphate-buffered solution and subsequently washed and submerged in phosphate-buffered saline to maintain the shape of the cells in their aqueous environment.

Figure 1 shows a Raman spectrum of the pure deuterated vesicles in aqueous environment. The spectrum is clearly dominated by the intensities of the C–D stretches of the aliphatic side chains between 2000 and 2310 $cm^{-1}$. Due to the nonpolar character of the bond, C–D stretching vibrations are an ideal candidate for large Raman intensities. All other peaks in the region between 650 and 1750 $cm^{-1}$ are of less intensity. The C–H stretches of the nondeuterated bonds of the phosphoester residue appear between 2800 and 3020 $cm^{-1}$. Spectra of pure vesicles in water were acquired as single position spectra at 2 s exposure. Images of vesicles could not be obtained due to the mobility of the particles in water (drying the particles onto the slides resulted in clumping).

Figure 2A shows a microscopic image of an MCF-7 cell incubated with LIP for 12 h at a concentration of 2 mg/mL. The image in Figure 2B was reconstructed from the Raman intensities of the C–H stretching region, reflecting different densities of different cellular components. Clearly discernible are the nucleus with nucleoli surrounded by the cytoplasm with varying density. High densities correspond to regions of high phospholipids content, looking like not yet shedded microparticles. The spectrum in Figure 3A represents a spectrum from within the cytoplasm, averaged over four adjacent data points to increase the signal-to-noise ratio. Spectra from the cytoplasm generally reflect its protein composition. The most pronounced Raman bands result from the C–H stretching vibrations between 2800 and 3020 $cm^{-1}$, the carbonyl stretches located around 1650 $cm^{-1}$, C–H bending deformations at 1450 $cm^{-1}$, and C–N bends of the peptide linkages between 1200 and 1400 $cm^{-1}$. Spectral differences of cellular components have been previously addressed and are therefore not discussed in detail.[1,3,5] The image in Figure 2C shows the Raman intensities of the C–D stretching vibrations for the same cell.

Apparently, after 12 h of incubation with deuterated LIP, a small fraction of these liposomes has become associated with cells, predominantly around the cell periphery, but also in some cytoplasmic areas. The image in Figure 2D is an overlay of the C–D and C–H intensities. An average spectrum from the red region, indicated by the arrow, is shown in Figure 3B. The intensities of the C–D vibrations are well pronounced between 2000 and 2300 $cm^{-1}$ and appear unaltered at the same spectral positions for free liposomes and the liposomes in cells. The C–D intensities within the region are still larger than the C–H intensities. The ratio of the two intensities generally varies for different positions within the red regions. All other Raman peaks of deuterated LIP couple with the protein bands, which was also observed for each individual spectrum of the region averaged over.

To ascertain that the liposomes are observed within the cytoplasm and not just adsorbed on the cell surface, a depth profile in the *xz*-direction was collected. The results shown in parts E–G of Figure 2 clearly indicate that the deuterated liposomes penetrate the cell body. The cell shown here is about 10 μm thick, which was found to be typical for this cell type. The spatial resolution for the employed laser is about 1 μm in the *z*-direction. The *xy*-image in Figure 2B was collected ca. 2 μm above the cell-substrate interface. The white bars indicate the scanning positions.

Figure 4 displays the Raman imaging results for 6, 12, 18, and 24 h of incubation, together with the bright field images of the individual cells. The second row shows the results for 12 h incubation for three cells. The regions where C–D intensities were detected appear as small droplet-like inclusions in all three cells, most of which are located around the cell edges. However, cell B2 also shows inclusions in the periphery of the nucleus, deep inside the cytoplasm. It is important to mention here that the uptake of plain LIP becomes reproducibly apparent in all observed cells only after approximately 12 h (note the virtual lack of the uptake in the images obtained after 6 h of incubation shown in row 1). Since the average scanning time for each cell is about 1 h it is difficult to obtain statistically reliable amounts of data. For each incubation time about 10 cells were imaged. After 12 h of incubation, all of the observed cells showed inclusions, whereas after 6 h inclusions were observed in only one cell. It is conceivable to assume that in between that time frame the overall uptake increases linearly until it reaches a plateau. However, the comparably small number of cells that can be scanned in reasonable time does not allow us to quantitatively proof this assumption. Rows 3 and 4 in Figure 4 show the overlaid images for 18 and 24 h incubation time. All cells exhibit inclusions of the deuterated phospholipids, generally on the order of a few microns in size, fully incorporated into the cell body. Interestingly, the amount of inclusions does not seem to vary with incubation time. In order to quantify the amount of deuterated phospholipids inside the cells, the ratios of the C–D vs the C–H intensities were calculated for each individual cell. The ratios for the cells are given in the lower right of each image. The values for the C–D and C–H intensities reflect the integrated areas between 2000 and 2300 $cm^{-1}$, within the red regions and 2800 and 3020 $cm^{-1}$ for the entire cell, respectively. The ratios vary between 0.005 and 0.02. Since Raman scattering intensities do not only vary with concentration, but also with density within the scattering volume, one has to be careful interpreting those values as percentages. Also, given a spatial resolution of 1 μm in the *z*-direction, only about 20% of the whole cell can be included in one image. However, the numbers provide a rough orientation, comparing the individual results.

Figure 5 shows the overlaid images for the uptake experiments using the TATp-LIP system for 3, 6, and 9 h of incubation. The data clearly demonstrate a significantly accelerated uptake of TATp-LIP. After just 3 h, large amounts of the deuterated TATp-LIP (partially aggregated) were found at the periphery of the cells around the cell membrane. After 6 h, TATp-LIP penetrated well into the cell body. Additional incubation for another 3 h did not increase the amount of deuterated phospholipids inside the cells. The associated C–D/C–H ratios are again given in the lower right of the Raman images. The ratios for the individual cells vary from 0.058 to 0.110. In comparison with the unmodified liposomes, the uptake was enhanced approximately by a factor 10. Cell C2 in Figure 5 exhibits inclusions around the edges as well as deeper inside the cytoplasm. The spectral plots in Figure 6 represent two average spectra from the areas indicated by the arrows. Noticeable is the reversal in intensity of the C–D and C–H stretches. The C–D/C–H ratio around the edges is greater than 1, and smaller than 1 inside the cell, which is also the case for the red regions inside cells C1 and C2, indicating less aggregation of the liposomes within the perinuclear region than around the cell edges. The distribution of liposomes may be diffusion controlled or regulated by intracellular trafficking processes. Little is known about fusion of phospholipids from liposomes with cellular membranes. Incorporation of lipids from nanoparticles into cell walls is limited.[21,22] However,

model studies have shown that lipid transfer between membranous vesicles is generally possible.[21,23] Perhaps over time phospholipids from liposomes fuse with phospholipids from intracellular membranes.

## Discussion

The most important result of our studies is that Raman microspectroscopy clearly allows for the observation of lipid particles uptake by the cells and their intracellular fate and distribution, thus providing a new mean to investigate fine details of the liposome-to-cell interactions. In this particulate case, we have also been able to compare the uptake efficiency for plain LIP and TATp-LIP. For both carrier systems, the uptake into the cells was clearly detected by Raman microspectroscopic measurements. The method applied showed also that upon the uptake, both systems apparently form aggregates larger in size than the spatial resolution, which is around 300 nm for the employed laser light.

Generally, liposome particles are taken up by endocytotic processes, which possibly lead to aggregation on the micrometer scale. That is especially the case for the TATp modified liposomes. Nanoparticles modified with cell penetrating peptides usually enter the cell by macropinocytosis.[15,16,24] However, Rayleigh scattering of very small particles can lead to spots of apparent size larger than the effective one. For the nonmodified liposomes some of the observed spots may actually be smaller than the theoretical spatial resolution. Confirming the previous experiments,[15] Raman microspectroscopy demonstrated significantly accelerated uptake of liposomes modified with TAT peptide compared with nonmodified liposomes– the uptake was clearly seen already after 3 h for TATp-LIP and only after 12 h for plain LIP. The CD/CH ratios from the imaging results for LIP vs TATp-LIP system can serve as a rough orientation to compare the amount of liposomes incorporated into the cytoplasm. The ratios for the LIP system were around the order of 0.01 and about 0.1 for the TATp modified particles. Again, these numbers can not be directly correlated to concentrations of incorporated liposomes or phospholipids. As already mentioned in the result section scattering intensities depend on the density of the molecular matrix within the scattering volume. However, given that the experiments for both systems were performed on the same cell line and on cells similar in size and thickness, the enhancement of cellular uptake of the TAT-peptide-modified liposomes can be estimated to be about 10-fold.

At the same time, the general pattern of the uptake and intracellular distribution of LIP and TATp-LIP were rather similar. The liposomal structures incorporated into the cells were in both cases initially found around the periphery (edges) of the cells. The initial aggregates seem to be larger in the case of TATp-LIP. With longer incubation times, more deuterated phospholipids accumulated in the perinuclear regions, although the overall amount did not change over the observed period of time as indicated by the CD/CH ratios. Since the employed lipid concentrations within the *in vitro* environment of the cells somewhat reflect an overdose, it is possible that the saturation is reached relatively quickly, certainly before the liposomal structures translocate within the cell body.

The spectral appearances of the C–D stretching region, with respect to band shapes and peak positions, did not change significantly upon uptake, indicating the lipid side chains did not undergo substantial conformational changes. However, a reversal of the C–D/C–H ratios for structures around the edges vs structures around the nucleus implies a wider distribution of DSPC-$d_{70}$ possibly due to exchange between incorporated phospholipids and phospholipids of intracellular membrane structures over time. We believe, Raman microspectroscopy can be successfully applied for the study of fine interactions of various pharmaceutical nanocarriers, including lipid-based nanocarriers, such as liposomes, within cells. The information obtained could allow for the optimization of the properties of such nanocarriers in a controlled fashion.

In principle, any organic molecule may be labeled with deuterium, which would also allow following the fate of cytotoxilogically active compounds that are potential candidates for these delivery systems.

All images were collected using the 488 nm line of the Argon ion laser. Although it is generally accepted wisdom that, for biological samples, excitation at higher frequencies of the visible spectrum causes fluorescence, none was observed for the cell type used in these experiments. Since the scattering intensity is proportional to the fourth power of the frequency, excitation in the blue and green range of the light spectrum offers enormous advantages over excitation in the red or near-infrared. This higher scattering cross section (by about a factor 6 between 785 and 488 nm excitation), along with significantly higher detector sensitivity and a better spatial resolution—due the shorter wavelength—markedly improves data quality.

## Acknowledgment

Partial support of this research from Grant No. CA 090346 (to M.D.), Grant No. CA121838 and HL55519 (to V.T.) and the IGERT nanomedicine education program (to T.C.) is gratefully acknowledged.

## References

1. Uzunbajakava N, Lenferic A, Kraan Y, Volokhina E, Vrensen G, Greve J, Otto C. Biophys. J 2003;84 (6):3968–3981. [PubMed: 12770902]
2. Matthäus C, Boydston-White S, Miljković M, Romeo M, Diem M. Appl. Spectrosc 2006;60(1):1–8. [PubMed: 16454901]
3. Matthäus C, Chernenko T, Newmark JA, Warner CM, Diem M. Biophys. J 2007;93:668–673. [PubMed: 17468162]
4. van Manen H, Kraan Y, Roos D, Otto C. Proc. Natl. Acad. Sci. U.S.A 2005;102(29):10159–10164. [PubMed: 16002471]
5. Krafft C, Knetschke T, Funk RHW, Salzer R. Anal. Chem 2006;78(13):4424–4429. [PubMed: 16808450]
6. Otto C, Sijtsema NM, Greeve J. Eur. Biophys. J 1998;27(6):582–589. [PubMed: 9791941]
7. Sijtsema NM, Otto C, Segers-Nolten IG, Verhoeven AJ. Biophys. J 1998;74(6):3250–3255. [PubMed: 9635778]
8. Sijtsema NM, Tibbe AG, Segers-Nolten IG, Verhoeven AJ, Weening RS, Greve J, Otto C. Biophys. J 2000;78(5):2606–2613. [PubMed: 10777757]
9. Torchilin VP. Nature Rev. Drug Discov 2005;4:145–160. [PubMed: 15688077]
10. Serpe L, Guido M, Canaparo R, Muntoni E, Cavalli R, Panzanelli P, Delia Pepal C, Bargoni A, Mauro A, Gasco MR, Eandi M, Zara GP. J. Nanosci. Nanotechnol 2006;6(9–10):3062–3069. [PubMed: 17048519]
11. Rao NM, Gopal V. Biosci. Rep 2006;26(4):301–324. [PubMed: 17029003]
12. Torchilin VP. Adv. Drug Deliv. Rev 2005;57(1):95–109. [PubMed: 15518923]
13. Huth US, Schubert R, Peschka-Suss R. J. Controlled Release 2006;110(3):490–504.
14. Gupta B, Levchenko T, Torchilin VP. Adv. Drug Deliv. Rev 2005;57:637–651. [PubMed: 15722168]
15. Wadia JS, Dowdy SF. Adv. Drug Deliv. Rev 2005;57(4):579–596. [PubMed: 15722165]
16. Torchilin VP. Ann. Rev. Biomed. Eng 2006;8:343–375. [PubMed: 16834560]
17. Dipali SR, Kulkarni SB, Betageri GV. J. Pharm. Pharmacol 1996;48(11):1112–1115. [PubMed: 8961156]
18. Liang W, Levchenko TS, Torchilin VP. J. Microencapsul 2004;21:151–161. [PubMed: 15198427]
19. Torchilin VP, Levchenko TS, Lukyanov AN, Khaw BA, Klibanov AL, Rammohan R, Samokhin GP, Whiteman KR. Biochim. Biophys. Acta - Biomembranes 2001;1511:397–411.
20. Ono A, Takeuchi K, Sukenari A, Suzuki T, Adachi I, Ueno M. Biol. Pharm. Bull 2002;25(1):97–101. [PubMed: 11824566]

21. Kristl J, Volk B, Ahlin P, Gombač K, Šentjurc M. Int. J. Pharm 2003;256:133–140. [PubMed: 12695019]
22. Wojewodzca J, Pazdzior G, Langner M. Chem. Phys. Lipids 2005;135(2):181–187. [PubMed: 15921977]
23. Palmerini CA, Cametti C, Sennato S, Gaudino D, Carlini E, Bordi F, Arienti G. J. Membr. Biol 2006;211:185–190. [PubMed: 17091211]
24. Wadia JS, Stan RF, Dowdy SF. Nature Med 2004;10:310–315. [PubMed: 14770178]

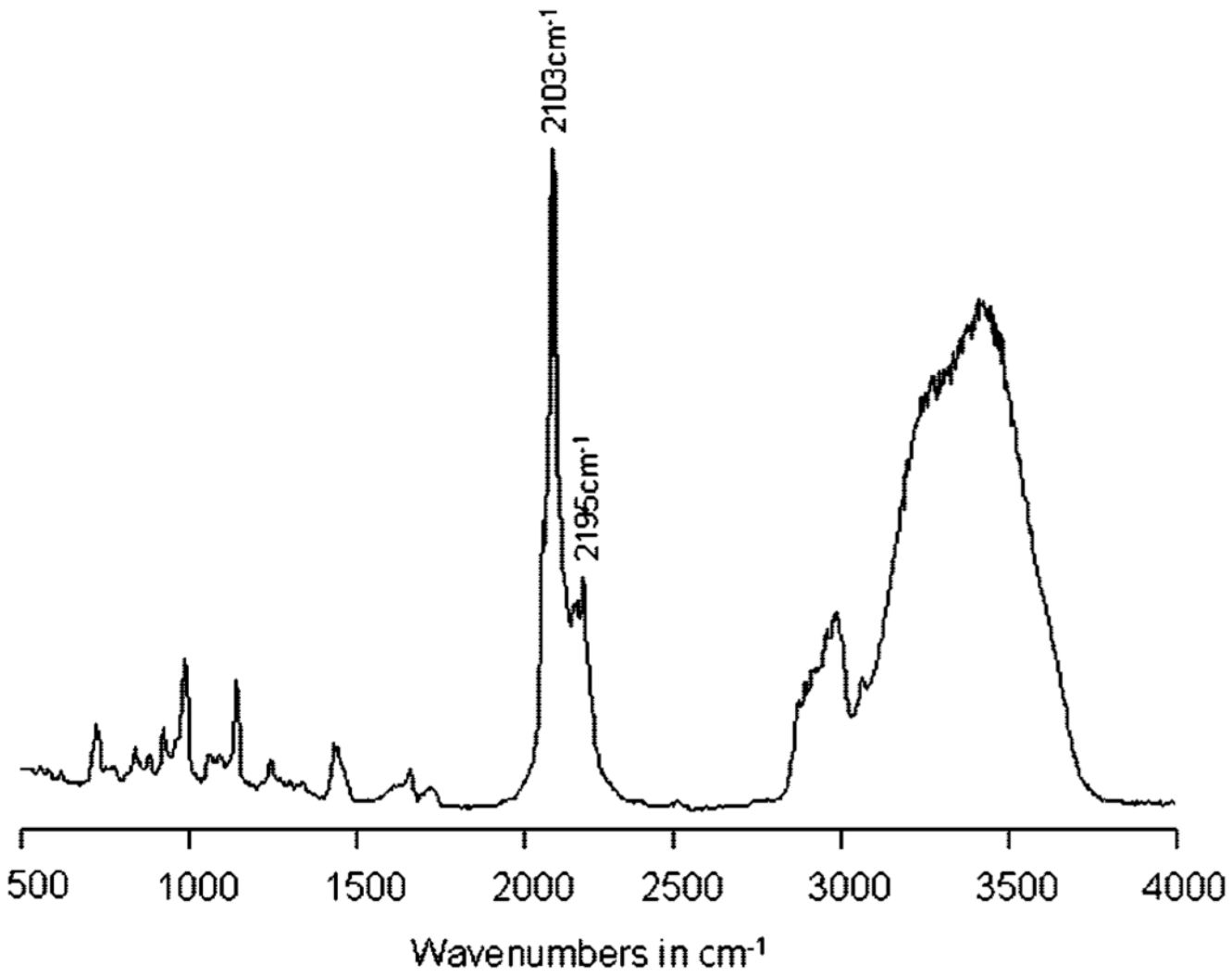


**Figure 1.**
Raman spectrum of deuterated DSPC-$d_{70}$ liposomes in aqueous environment.

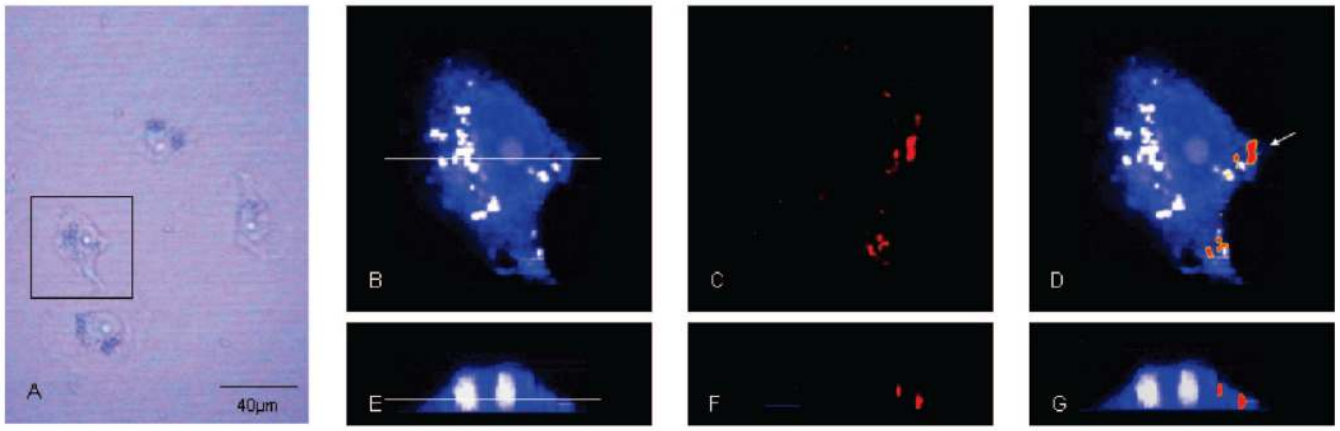


**Figure 2.**
MCF-7 cells treated with DSPC-$d_{70}$ liposomes at 2 mg/mL for 12 h (A). Raman images of one cell reconstructed from the C–H (B) and C–D stretching intensities (C). The image in (D) represents an overlay of panels (B) and (C). A depth profile was collected for the same cell (E–G). Scanning positions are indicated by the white bar.

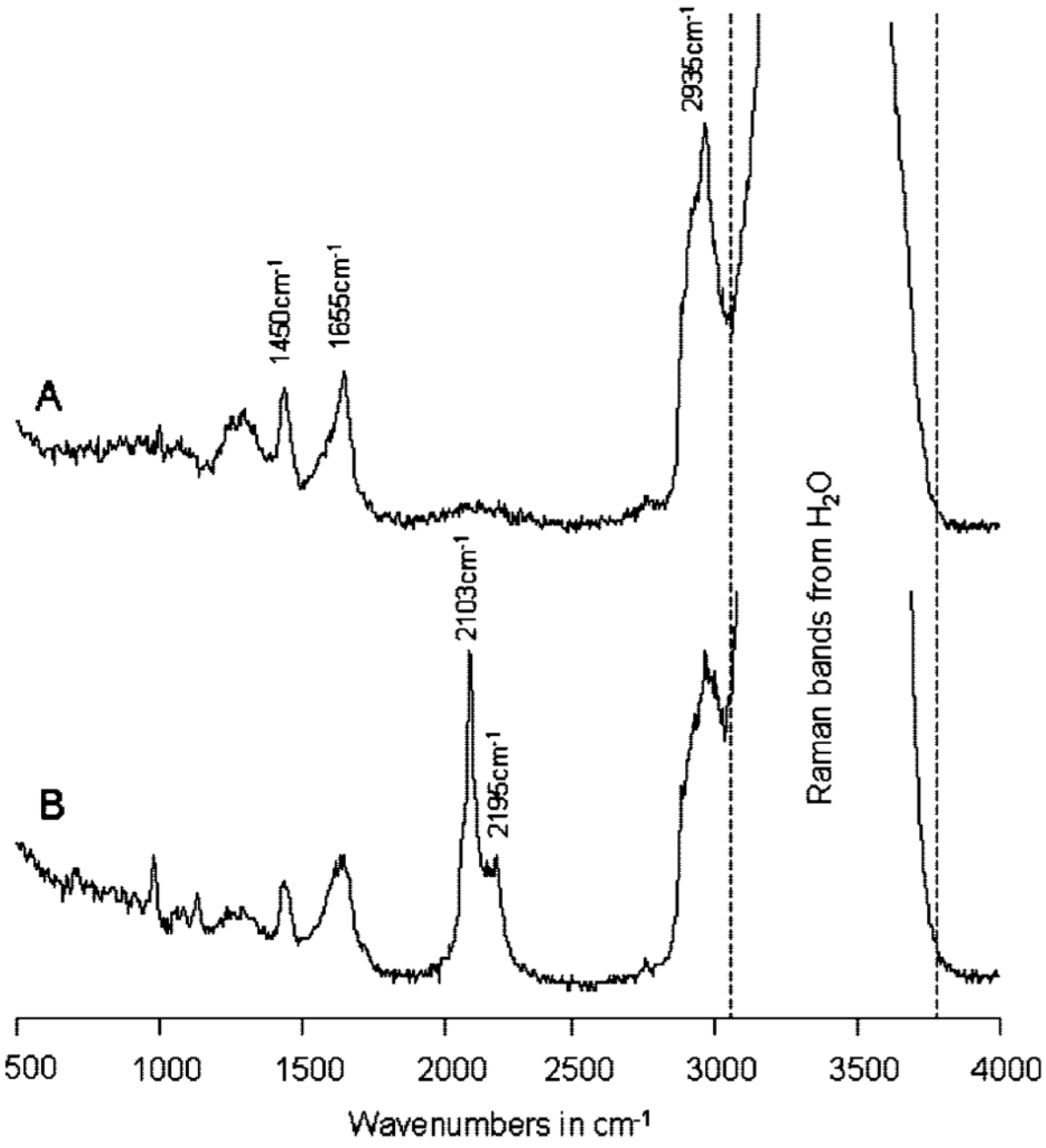


**Figure 3.**
Typical Raman spectrum from within the cytoplasm (A) with characteristic protein bands, and a spectrum from DSPC-$d_{70}$ liposomes inside the cell with strong C–D stretching intensities (B).

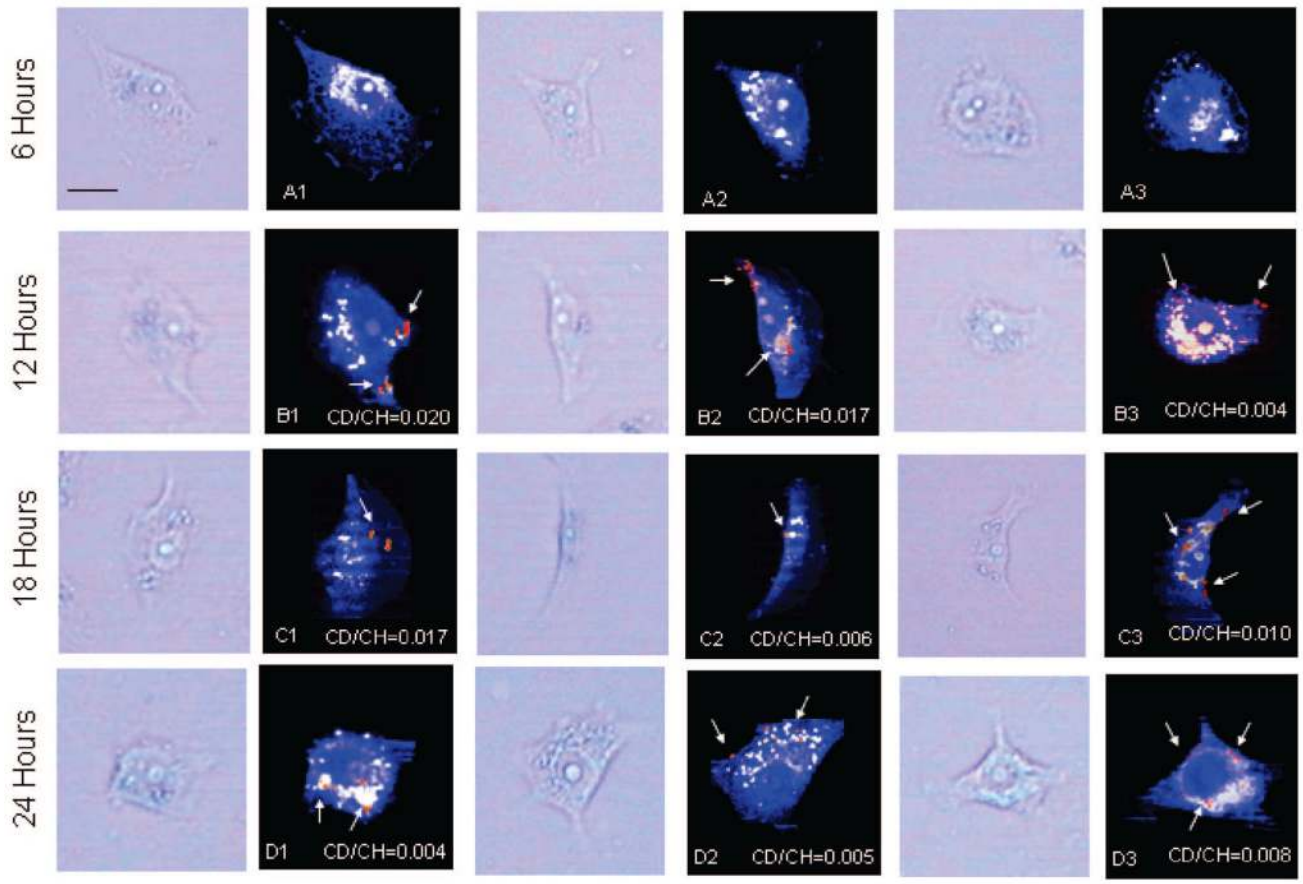


**Figure 4.**

Bright field images and Raman images from MCF-7 cells inoculated with DSPC-$d_{70}$ liposomes for 6, 12, 18, and 24 h. Raman images were reconstructed from the C–H stretching intensities between 2800 and 3020 $cm^{-1}$. C–D stretching intensities between 2000 and 2310 $cm^{-1}$ are shown in red. The CD/CH intensity ratios for the individual cells are given in the lower right of each picture. The scale bar is 20 μm.

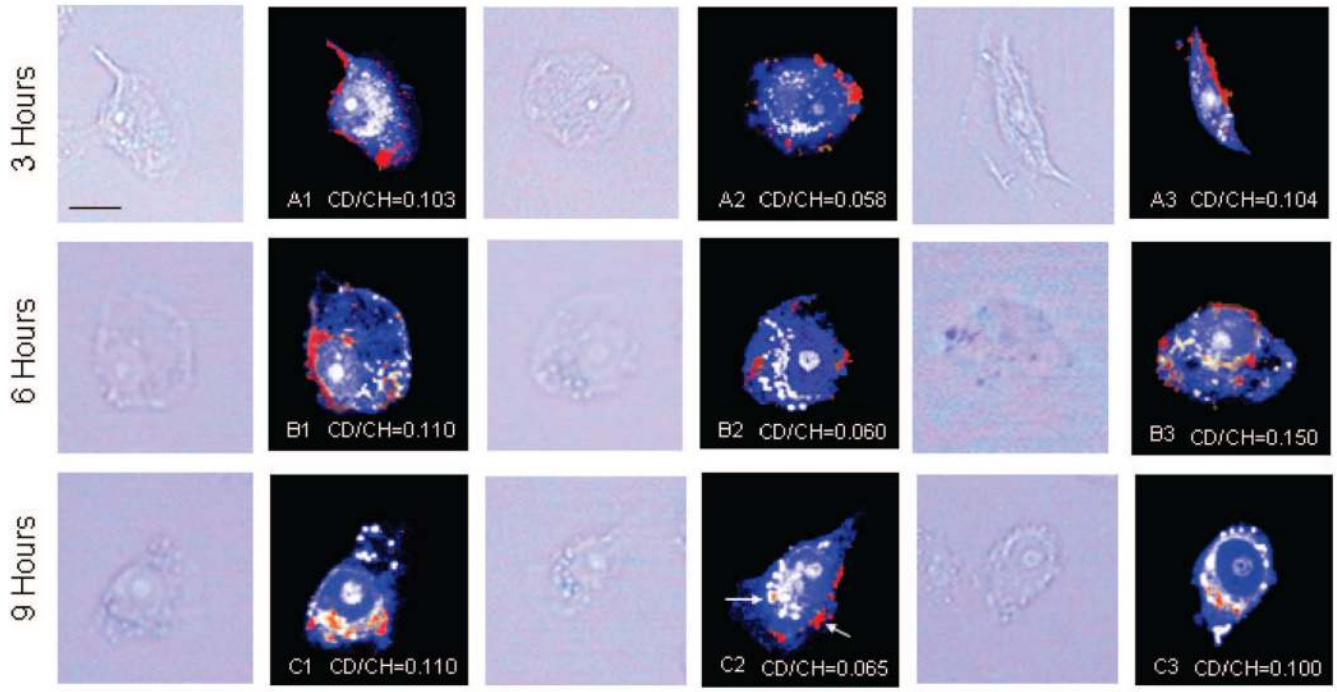


**Figure 5.**

Bright field images and Raman images from MCF-7 cells inoculated with DSPC-$d_{70}$ TAT-peptide modified liposomes for 3, 6, and 9 h. Raman images were reconstructed from the C–H stretching intensities between 2800 and 3020 $cm^{-1}$. C–D stretching intensities between 2000 and 2310 $cm^{-1}$ are shown in red. The CD/CH intensity ratios for the individual cells are given in the lower right of each picture. The scale bar is 20 μm.

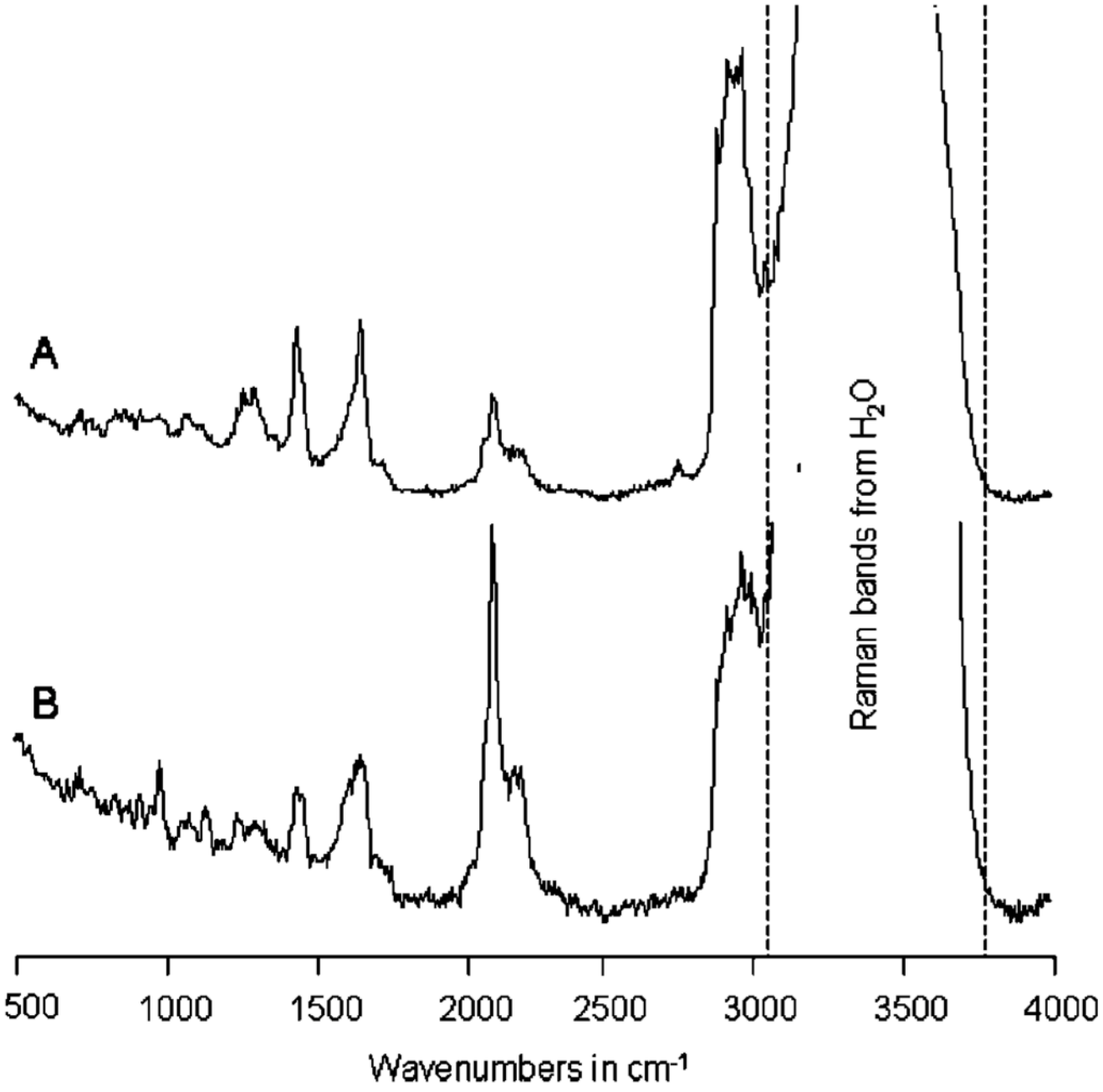


**Figure 6.**
Average Raman spectra from within a region around the edges of cell C2 in Figure 5A in comparison with a spectrum from a region in the periphery of the nucleus of the same cell (Figure 5B).